Local and global properties of light-bound atomic lattices investigated by Bragg diffraction

Matthias Weidemüller,* Axel Görlitz, Theodor W. Hänsch, and Andreas Hemmerich†
Sektion Physik, Universität München, Schellingstraße 4/III, D-80799 München, Germany
and Max-Planck-Institut für Quantenoptik, D-85748 Garching, Germany
(Received 14 May 1998)

We explore Bragg diffraction from atomic lattices bound by light as a diagnostic tool for studying properties of optical lattices not accessible so far. A weak laser beam at a wavelength of about half the wavelength of the lattice field is diffracted from the (100) and (130) lattice planes of a Rb optical lattice. The observation of well-defined Bragg spots confirms the long-range order in optical lattices. From the acceptance angle for Bragg diffraction we deduce the range over which crystalline order is preserved. The comparison of two Bragg spots diffracted from different lattice planes allows us to directly measure the position spread of the atomic wave packets oscillating in the light-induced potential wells. By combining conventional probe transmission spectroscopy with Bragg diffraction we study the motion of atoms that are deeply bound inside the potential wells. We show experimentally and theoretically how backaction of the bound atoms on the trapping field influences the lattice constant. We develop a model for the modification of the refractive index by the highly ordered atomic medium. Based on first-order scattering theory the model explicitly includes the influence of atomic localization on the resulting lattice constant. By measuring the change of the Bragg angle, we observe a decrease of the lattice plane separation for increasing atomic density. We report experimental evidence for the correction to the refractive index due to the finite position spread of the atoms. [S1050-2947(98)05611-X]

PACS number(s): 42.25.Fx, 32.80.Pj, 42.65.−k

I. INTRODUCTION

Atoms subjected to standing light waves with specifically designed spatial patterns of the intensity and the polarization differ significantly from conventional samples of laser-cooled atomic gases [1]. The atoms no longer move ballistically but are trapped in micropotentials created by the ac Stark effect, originating from the interaction of the light field with the induced atomic dipole. The potentials form a regular, periodic structure for which, in the ideal case, symmetry will be preserved over the entire extension of the light field. Bound at definite sites the atoms form a highly ordered structure called an *optical lattice*. Under these circumstances the quantization of the atomic center-of-mass (c.m.) motion becomes important, giving rise to discrete vibrational levels. Sub-Doppler cooling mechanisms prepare a nearly thermal distribution of the atoms among these levels at temperatures of a few tens of microkelvin, where most atoms are trapped in the lowest few states [2,3]. The lattice constant in optical lattices is determined by the optical wavelength and thus is three orders of magnitude larger than the lattice constants of crystals. Hence, fundamental phenomena well known from solid state and condensed matter physics can be fruitfully studied in a novel regime. Prominent examples are the indication of paramagnetic behavior in light-bound atomic lattices [4], demonstration of analogies to the photorefractive effect [5], and the realization of quasiperiodic optical lattices [6]. By accelerating one-dimensional optical lattices, Bloch waves and Wannier-Stark ladders could be experimentally studied in a regime unaccessible in condensed matter systems [7].

Bragg diffraction in optical lattices has been reported independently by two research groups, namely, the group of Phillips at NIST in Gaithersburg [8] and our group [9]. It became possible to extract direct information on the long-range order imposed by the lattice field on the ultracold atomic sample. As schematically shown in Fig. 1, the requirements for Bragg diffraction in optical lattices differ from the ones in the regime of x-ray diffraction crystallography. Since the lattice constants are on the order of optical wavelengths, monochromatic laser light can be used for

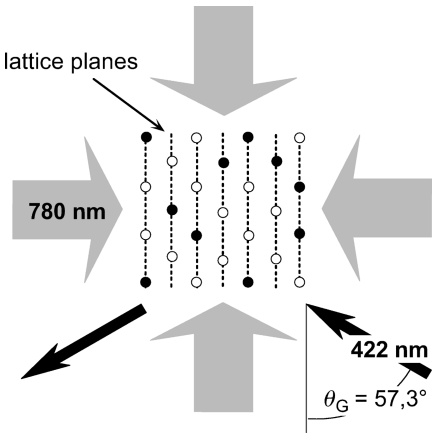

FIG. 1. 2D schematic presentation of Bragg diffraction from optical lattices. The atomic lattice is formed in the intersection of six laser beams, with the pair of laser beams perpendicular to the drawing plane not shown here. The lattice constant is determined by the wavelength of the lattice field ($\lambda_L = 780$ nm). Occupied lattice sites are represented by filled circles. A laser beam of shorter wavelength ($\lambda_B = 422$ nm) is diffracted from the lattice planes when the Bragg condition is fulfilled.

*Present address: Max-Planck-Institut für Kernphysik, Postfach 10 39 80, 69029 Heidelberg, Germany.
†Present address: Institut für Laserphysik, Universität Hamburg, Jungiusstrasse 9, 20355 Hamburg, Germany.

Bragg diffraction. The scattering process responsible for the diffraction is resonant elastic Rayleigh scattering from the bound atoms.

In our experiments the incident probe beam for Bragg diffraction operates near a transition to a higher excited atomic state at a frequency nearly twice the lattice field frequency. The interference between the lattice field and the Bragg beam then oscillates so rapidly that it has no effect on the atoms. Otherwise additional undesired four-wave-mixing processes can arise [10,11], which obscure Bragg diffraction [12]. Since in the experiments presented here the optical lattice is not perturbed by the Bragg diffraction, the lattice properties can be studied *in situ*. An alternative, but destructive method to distinguish Bragg diffraction from four-wave mixing was successfully demonstrated by Birkl *et al.* [8] who have used nearly the same frequency for Bragg diffraction as for the generation of their optical lattice. In their experiment, the lattice beams were quickly turned off, and the Bragg diffracted light was monitored before the lattice had enough time to decay. Observed decay times were on the order of microseconds.

One might wonder if the present low filling factors in optical lattices corresponding to approximately 99% vacancies do not prevent the observation of Bragg diffraction. In contrast to crystals, vacancies in dilute optical lattices do not distort the lattice geometry, which is to zeroth order determined by the lattice field only. The low filling factors of conventional optical lattices thus do not impede Bragg diffraction but may lead to additional diffuse scattering. Despite this diffuse scattering, the power coherently scattered into the Bragg directions exceeds the background incoherently scattered into the same solid angle by orders of magnitude.

While spectroscopic techniques (e.g., stimulated Raman spectroscopy [13] or fluorescence spectroscopy [14]) have provided much information on the dynamics of each atom at its specific lattice site, our knowledge concerning their collective behavior has been quite restricted. Although the atomic densities achieved so far are still too low to expect much interaction between atoms located at different lattice sites, hopes are raised to reach this goal in the future [15]. In such strongly populated lattices one could observe collective interactions and quantum correlations of matter waves in a strongly confined system [16]. Our work is inspired by the desire to explore novel tools that let us study long-range order aspects.

As an example for the subtle interplay between the light field creating the lattice and the atoms acting as a polarizable medium we investigate the change of the lattice plane separation as a function of the atomic density. At sufficiently high densities the backaction of the atoms on the lattice field becomes significant and influences the lattice geometry. To first order, the atoms are characterized by a refractive index that modifies the spacing of adjacent lattice planes proportionally to the atomic density. We will show that this modification is significantly enhanced by the fact that the atoms are strongly localized inside the potential wells.

In this paper we give a detailed description of our recent work on the application of Bragg diffraction to optical lattices [9,17]. Special emphasis is posed on the use of Bragg diffraction as a versatile technique for the investigation of important static and dynamic properties of optical lattices. Section II presents the conceptual basis for the understanding of our experiments. The crystallographic structure of the lattice is discussed in Sec. II A. Coherent and incoherent contributions to the Bragg diffracted power are identified, and the Debye-Waller factor for the optical lattice is introduced in Sec. II B. Section II C is devoted to a simple model for the change of the refractive index due to the presence of a highly ordered sample of localized atoms. Section III describes important components of our Bragg diffraction experiment: the magneto-optical trap used to load the lattice, the lattice field configuration, the diode-laser–based source generating blue light for the Bragg diffraction, and the detection of different Bragg peaks. Results of our measurements are presented in Sec. IV. The relevance of Bragg diffraction for the study of long-range order is discussed in Sec. IV A. Measurements of the acceptance angle presented in Sec. IV B yield the range over which periodic order is preserved. The comparison of Bragg peaks from different lattice planes allows a precise determination of the extension of the atomic wave packets bound in the potential wells via the Debye-Waller factor, as shown in Sec. IV C. Using the independently determined values of the lattice extension and the Debye-Waller factor, the number of atoms actually ordered in the lattice is deduced from the measured absolute diffracted power in Sec. IV D. A kind of probe spectroscopy is described in Sec. IV E, complementing conventional transmission and fluorescence spectroscopy to study atomic motion in the potential wells. By precisely mapping out the Bragg condition for various densities we determine experimentally the change of the lattice constant and elucidate the importance of the atomic localization on this effect in Sec. IV F. Finally, in Sec. V the results are discussed in view of future applications.

II. GENERAL CONSIDERATIONS

A. Structure of the lattice

A spin-polarized atomic lattice is created in the intersection of three mutually orthogonal standing light waves [Fig. 2(a)]. As will be explained in Sec. III B our experimental apparatus allows us to switch between different lattice geometries. We will concentrate on the two lattice geometries shown in Fig. 2, which belong to the groups of simple tetragonal (st) [Fig. 2(b)] and of body-centered-cubic (bcc) [Fig. 2(c)] Bravais lattices, respectively [18].

We characterize the lattice structure by a conventional cubic cell with a basis consisting of two atoms at positions $\mathbf{d}_1=(0,0,0)$ and $\mathbf{d}_2=(\lambda_L/2)\,(1,1,1)$ for the bcc structure, and four atoms at $\mathbf{d}_1=(0,0,0)$, $\mathbf{d}_2=(\lambda_L/2)\,(1,1,0)$, $\mathbf{d}_3=(\lambda_L/2)\,(0,0,1)$ and $\mathbf{d}_4=(\lambda_L/2)\,(1,1,1)$ for the st structure. λ_L is the wavelength of the lattice field ($\lambda_L=780.2$ nm in our case). The primitive cubic unit cell is spanned by the vectors $\mathbf{a}_j=\lambda_L\mathbf{e}_j$, $j=x,y,z$, where the $\mathbf{e}_j$ denote the Cartesian unit vectors along three orthogonal lattice beams. A basis of the reciprocal lattice is then defined by the vectors $\mathbf{b}_j=k_L\mathbf{e}_j$, where $k_L=2\pi/\lambda_L$. As a general property of optical lattices, the reciprocal-lattice vectors $\mathbf{G}$ can always be expressed as linear combinations of the wave vectors of the light beams used to form the lattice [19].

Bragg diffraction occurs when the difference $\Delta\mathbf{k}$ between the incident and the diffracted wave vector equals a recipro-

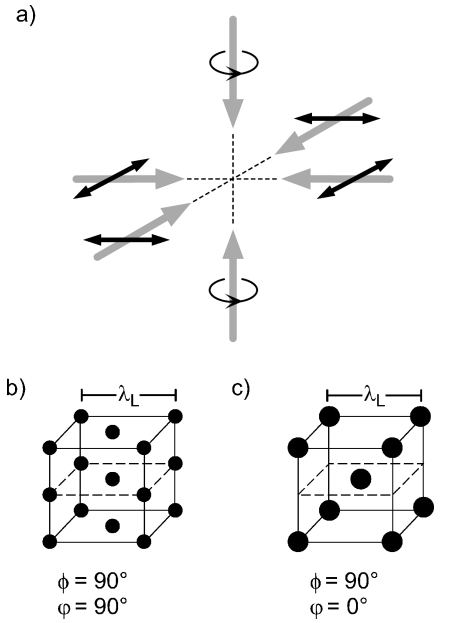

FIG. 2. (a) Field configuration and (b),(c) unit cells for our six-beam optical lattice at wavelength λ_L for different time phase differences. The relative time phase difference between the two linearly polarized standing waves in the horizontal plane is denoted by ϕ, while φ is the time phase difference of the circularly polarized vertical standing wave with respect to the horizontal ones. The size of the dots indicates the depth of the optical potentials.

cal lattice vector **G**, i.e., $\Delta\mathbf{k}=\mathbf{G}\equiv\Sigma_i m_j\mathbf{b}_j$ where the m_j's are integers. This is equivalent to Bragg's law

$$2d_{\mathbf{G}}\cos\,\theta_{\mathbf{G}}=\lambda_B, \tag{1}$$

where $\theta_{\mathbf{G}}$ denotes the angle between the incident wave vector and the normal on the lattice plane given by **G**. The wavelength of the diffracted light is given by λ_B, and $d_{\mathbf{G}}=2\pi/|\mathbf{G}|$ is the spacing between the lattice planes.

Since the basis of the unit cell consists of two (bcc) and four (st) atoms, respectively, the possible combinations of the m_j's are restricted. For the bcc structure, the condition for constructive interference requires the sum $\Sigma_j m_j$ to be an even integer, whereas for the st structure the sum and additionally m_3 have to be even numbers. Since the incident beam is monochromatic the number of possible diffraction peaks is limited by the condition $|\mathbf{G}|\leqslant 2k_B$ where $k_B=2\pi/\lambda_B$ denotes the wave number of the incident beam. If we restrict ourselves to an incident light beam propagating within the x-y plane (i.e., $m_3=0$) we find four possible Bragg diffraction geometries ($\lambda_B=421.7$ nm in our case) originating from three families of equivalent lattice planes. While from the (100) and (130) planes only second or, respectively first order scattering may be observed, first- and second-order scattering is possible from the (110) planes [we use the Miller indices (m_x,m_y,m_z) to characterize the lattice planes [18]]. The possible directions for Bragg diffraction can be determined by Eq. (1). In the experiments described in this paper we concentrate on Bragg diffraction from the (100) and the (130) lattice planes of the body-centered-cubic lattice. The corresponding geometries are depicted in Fig. 3.

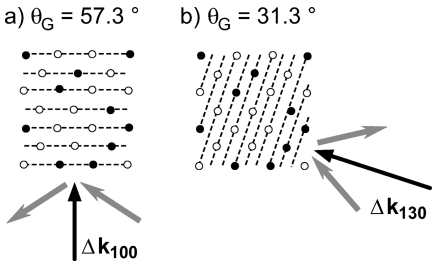

FIG. 3. Geometries for Bragg diffraction from the (100) (a) and (130) (b) lattice planes. $\Delta\mathbf{k}_{100}$ and $\Delta\mathbf{k}_{130}$ denote the different scattering vectors for Bragg scattering. Angles and lengths of the scattering vectors are drawn to scale.

B. Bragg diffraction

If the atoms occupy mainly the lowest-lying vibrational levels the optical potential wells are essentially harmonic. The potentials considered in this article are isotropic and can thus be characterized by a single vibrational frequency ω_{vib}. The unit cells of the lattice are assumed to be situated at sites **R**. From the N lattice sites available only N_* are actually occupied by an atom. For the near-resonant optical lattices investigated here, N_*/N is typically on the order of 10^{-2}.

Consider a linearly polarized plane traveling wave with intensity I to be incident on the atomic lattice. The scattering amplitude A_s for elastic Rayleigh scattering from a single atom is given by

$$A_s=\frac{\pi}{\lambda_B^2}\sqrt{I}\,\sin(\xi)|\alpha|, \tag{2}$$

where ξ is the angle between the diffracted wave vector and the polarization vector of the incident beam, and α denotes the product between the polarizability tensor and the incident polarization vector.

We assume N_* atoms to be randomly distributed among N available lattice sites, where N equals the number of unit cells for the cubic Bravais lattice multiplied by the number of sites per unit cell. The power dP scattered into the solid angle $d\sigma$ is then given by [20]

$$\frac{dP}{d\sigma}=\left(\frac{N_*}{N}\right)^2|A_s|^2\left(\beta^2|S|^2\left|\sum_{\mathbf{R}}e^{i\Delta\mathbf{k}\cdot\mathbf{R}}\right|^2+N(1-\beta^2)+\frac{N(N-N_*)}{N_*}\right), \tag{3}$$

where β denotes the Debye-Waller factor and $S=\Sigma_\nu\exp(i\Delta\mathbf{k}\cdot\mathbf{d}_\nu)$ is the structure factor of the unit cell.

Let us discuss the different contributions to the scattered power in Eq. (3). The first term represents the coherent scattering contribution. It is reduced by the square of the filling factor $(N_*/N)^2$ as compared to what one would expect for a completely filled lattice. The sum in this term has to be taken over all available unit cells. Only if $\Delta\mathbf{k}$ satisfies the Bragg condition does this term yield a contribution to the scattered power that scales with N_*^2 as expected for coherent scattering.

The atomic c.m. motion inside the potential wells reduces the coherent scattering contribution which is described by

the Debye-Waller factor $\beta=\overline{\exp(i\Delta\mathbf{k}\cdot\mathbf{x})}$ where $\mathbf{x}$ denotes the actual position of the atom's c.m. and the bar indicates the average over the distribution of $\mathbf{x}$ [21]. The atomic c.m. wave function can be characterized by a root-mean-square (rms) deviation $\delta R_\swarrow=[\overline{(x_\swarrow-R_\swarrow)^2}]^{1/2}$, where $\swarrow=X,Y,Z$ indicate the axis of an arbitrary Cartesian coordinate system. For the distribution of $\mathbf{x}$ we assume a Gaussian centered at the lattice site. In a harmonic oscillator potential this assumption is fulfilled for a thermal energy distribution. In this case, the Debye-Waller factor can be expressed in the simple form $\beta=e^{-W}$ with the exponent W given by

$$W=\frac{1}{2}\sum_{\swarrow=X,Y,Z}(\Delta k_\swarrow)^2(\delta R_\swarrow)^2. \tag{4}$$

Hence, an increase in temperature, corresponding to an increasing mean displacement of the atoms from the minima of the potential wells, decreases the scattering amplitude [22]. When all the $\delta R_\swarrow$ are the same (isotropic potentials), Eq. (4) simplifies to $W=\frac{1}{6}(\Delta\mathbf{k})^2(\delta R)^2$ with the rms extension δR given by $\delta R\equiv(\Sigma_\swarrow\delta R_\swarrow^2)^{1/2}$.

The second term in Eq. (3) is related to the background of incoherently scattered light. In addition to the reduction of the scattering amplitude, the motion inside the potential wells gives rise to an incoherent background that scales with N_*^2/N [20].

The third term in Eq. (3) describes another incoherent contribution resulting from the random distribution of the atoms among the lattices sites. If all lattice sites were occupied (i.e., $N_*=N$) this term would vanish. For the realistic case $N_*\ll N$ its contribution is proportional to the number of irradiated atoms N_* and can therefore still be neglected with respect to the first term (proportional to N_*^2) if N_* is sufficiently large.

If no crystalline order is present (i.e., $\beta=0$), we find that the total scattered power is completely incoherent and is simply given by $N_*|A_s|^2$. Other sources of additional background, for example, possible contributions from a fraction of nonordered atoms, are not treated here. Since the scattered power associated with such incoherent processes always scales with the number of atoms to the first power these processes will not obscure the appearance of well-defined Bragg spots. For all practical considerations we can therefore neglect the incoherent contributions.

C. Atomic backaction on the lattice field

If one approaches the case where all lattice sites are occupied by an atom, one certainly may no longer neglect the effect of the atoms on the near-resonant lattice beams and the effect of light-induced mutual interactions. In order of their appearance with increasing density these interactions are phase effects that distort the lattice field [23], multiple photon-scattering processes involving two or more atoms that lead to interatomic forces [24,25], van der Waals interactions, and finally phenomena of quantum statistical nature when more than one atom is bound inside a potential well [16]. The highest atomic densities reached in conventional optical lattices nowadays allow us solely to identify interactions of the first kind.

The trapping and cooling mechanisms that bind the atoms in the lattice sensitively rely on the polarizations of the lattice beams. These, in turn, depend on the phases accumulated by the light while passing through the atomic medium. Thus, we may expect a complex self-organization process that involves nonlocal interactions in the sense that the force exerted on some atom may depend on the atomic medium at some distant location [26]. To study the regime where this self-formation process develops its full richness is a challenging task: experimentally, because relatively dense atomic samples are required, and theoretically, because of its extreme complexity. However, to lowest order a quite simple model is applicable, which treats the atoms as an inhomogeneously distributed medium characterized by an index of refraction. In this simple picture, we only account for first order scattering of the lattice beams from the periodically arranged atoms. We will see that long-range order and localization yield an effective refractive index strongly differing from the case of a homogeneously distributed gas.

Since the optical lattices treated here operate at negative detuning with respect to the atomic resonance frequency the index of refraction is larger than one. This results in a reduced effective optical wavelength and thus a contraction of the lattice. The degree of atomic localization as described by the Debye-Waller factor influences the change of the refractive index. The better the atoms are localized the more strongly the lattice contracts.

In the following we will derive an expression for the lattice contraction. For this purpose we calculate the refractive index experienced by the lattice beams. Knowing the refractive index we can then determine the change of the lattice constant due to the presence of the atoms. A refractive index n larger (smaller) than one will lead to a smaller (larger) spacing between lattice planes $d_{\mathrm{eff},\mathbf{G}}=2\pi/(n|\mathbf{G}|)$. This can readily be measured by a change of the Bragg scattering angle, since the deviation $\Delta\theta_\mathbf{G}$ from the Bragg angle $\theta_\mathbf{G}$ as defined by Eq. (1) is given by

$$\Delta\theta_\mathbf{G}\simeq-(n-1)\cot\theta_\mathbf{G} \tag{5}$$

and is thus proportional to the atomic density.

Generally, the optical lattice is formed by M traveling light beams $\mathbf{E}_\mu(\mathbf{r})=\hat{\boldsymbol{\epsilon}}_\mu E_\mu\exp(i\mathbf{k}_\mu\cdot\mathbf{r})+\text{c.c.}$, where $1\leqslant\mu\leqslant M$. Here, $\hat{\boldsymbol{\epsilon}}_\mu$ is a complex normalized polarization vector, E_μ denotes the spatially constant complex field amplitude of the beam μ, and $|\mathbf{k}_\mu|\equiv k_L=2\pi/\lambda_L$. We wish to calculate the total field $\mathbf{E}_{\alpha,\mathrm{scatt}}(\mathbf{r})$ scattered into the direction $\mathbf{k}_\alpha$ with polarization $\hat{\boldsymbol{\epsilon}}_\alpha$ by taking only first-order scattering into account. This assumption certainly holds in the case of sparsely populated optical lattices. Since the wave vectors $\mathbf{k}_\mu$ constitute Bravais vectors of the reciprocal lattice we expect contributions from other lattice beams $\mu\neq\alpha$ arising from coherent scattering of the beam μ into the beam α in addition to the usual forward-scattering contribution resulting from $\mathbf{E}_\alpha$.

For simplicity, we assume in the following that the lattice provides only a single type of lattice site and posseses complete periodic order with respect to all wave vectors $\mathbf{k}_\mu$ that represent a basis of the reciprocal lattice. This is fulfilled for all spin-polarized four- and six-beam geometries. As an implication of this assumption the polarizability tensor $\vec{\alpha}_\mathbf{R}$ is the same at all lattice sites $\mathbf{R}$. In order to derive the first-

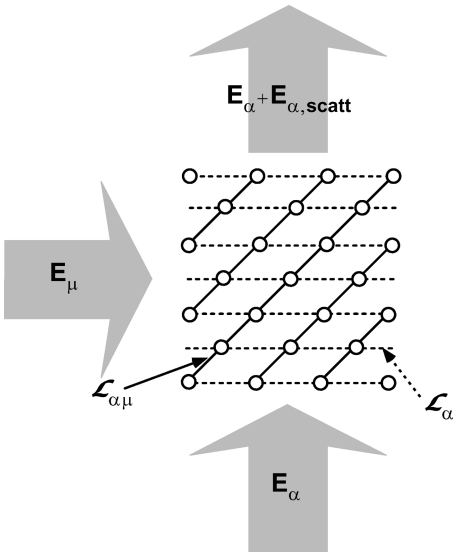

FIG. 4. Scheme for the enhancement of the refractive index due to scattering from an ordered ensemble of localized atoms. The refractive index as seen by the incoming wave $\mathbf{E}_\alpha$ is enhanced by scattering of the wave $\mathbf{E}_\mu$ into the direction of $\mathbf{E}_\alpha$. The scattered wave $\mathbf{E}_{\alpha,\mathrm{scatt}}$ is thus formed by components from forward scattering of $\mathbf{E}_\alpha$ at the planes $\mathcal{L}_\alpha$ as for a dilute sample and from 90° scattering of $\mathbf{E}_\mu$ at the planes $\mathcal{L}_\alpha\mu$.

order scattering contribution from the μth beam we consider all atomic dipoles induced by $\mathbf{E}_\mu$ and arranged on the Q contributing lattice planes $\mathcal{L}_{\alpha\mu}^{(q)}$, $1\leqslant q\leqslant Q$, perpendicular to the reciprocal lattice vector $\mathbf{k}_\alpha-\mathbf{k}_\mu$, and calculate the plane wave emitted into the $\mathbf{k}_\alpha$ direction [27] (see Fig. 4).

In the optical lattice the atoms are arranged such that all dipoles contribute coherently since the condition for Bragg scattering from one trapping beam into the other is automatically fulfilled. Therefore, the spatial phase of the emitted plane wave depends only on the position of a single lattice site $\mathbf{x}^{(q)}$, which represents the entire lattice plane. The scattered amplitude scales with the atomic area density $\eta_{\alpha\mu}$ of the lattice plane $\mathcal{L}_{\alpha\mu}$ divided by the cosine of half the scattering angle $\theta_{\alpha\mu}$. The term $\eta_{\alpha\mu}\cos\theta_{\alpha\mu}/2$ is equal to the atomic area density η_α of the lattice plane $\mathcal{L}_\alpha$ perpendicular to $\mathbf{k}_\alpha$. We choose the same lattice site at position $\mathbf{x}^{(q)}$ as a representative for all different kinds of lattice planes $\mathcal{L}_{\alpha\mu}$ connected with different values of μ and take the sum over all corresponding scattering contributions. We then have to take the sum over all contributing lattice planes along the direction $\mathbf{k}_\alpha$, thus finding that the total scattered field is

$$\mathbf{E}_{\alpha,\mathrm{scatt}}(\mathbf{r})=\frac{i}{2}\mathbf{E}_\alpha(\mathbf{r})\varepsilon_0 k_L\eta_\alpha\sum_\mu\frac{E_\mu}{E_\alpha}\times\sum_q(\hat{\boldsymbol{\epsilon}}_\alpha^*\vec{\alpha}_{\mathbf{x}}^{(q)}\hat{\boldsymbol{\epsilon}}_\mu)e^{i(\mathbf{k}_\mu-\mathbf{k}_\alpha)\cdot\mathbf{x}^{(q)}},\qquad(6)$$

where ε_0 is the dielectric constant in vacuum.

We account for the imperfect localization of the atoms by assuming that the position vectors in the second sum of Eq. (6) can be written as $\mathbf{x}^{(q)}=\mathbf{R}+\delta\mathbf{R}$ where $\mathbf{R}$ denotes a real lattice site $[\exp[(\mathbf{k}_\mu-\mathbf{k}_\alpha)\cdot\mathbf{R}]=1]$ and $\delta\mathbf{R}$ is a small random deviation that follows a Gaussian distribution. Similar to the derivation of Eq. (4), we then express the average of the sum over q by the product $Q\beta_{\alpha\mu}$. As in Sec. II B the exponent $W_{\alpha\mu}$ of the Debye-Waller factor $\beta_{\alpha\mu}=e^{-W_{\alpha\mu}}$ corresponding to the lattice plane $\mathcal{L}_{\alpha\mu}$ is given by $W_{\alpha\mu}=\frac{1}{6}(\mathbf{k}_\mu-\mathbf{k}_\alpha)^2(\delta R)^2$ for isotropic potentials.

We assume that the density $\varrho=Q\eta_\alpha/\lambda_L$ is sufficiently low such that the refractive index n_α experienced by the lattice beam along $\mathbf{k}_\alpha$ is close to unity. Using Eq. (6) we derive the refractive index by calculating the phase accumulated by the beam α. This procedure gives the expression

$$n_\alpha-1=\frac{1}{2}\varepsilon_0\varrho\sum_\mu\frac{E_\mu}{E_\alpha}(\hat{\boldsymbol{\epsilon}}_\alpha^*\vec{\alpha}_{(\mathbf{R})}\hat{\boldsymbol{\epsilon}}_\mu)\beta_{\alpha\mu}.\qquad(7)$$

For a homogeneously distributed gas without atomic localization (i.e., $\beta_{\alpha\mu}=\delta_{\alpha\mu}$ with δ denoting the Kronecker function) we get the well-known result that only forward scattering yields a contribution to the refractive index. In bright optical lattices, which typically trap the atoms in the intensity antinodes, the sum of all Bragg-scattering contributions (i.e., $\alpha\neq\mu$) adds to the forward scattering term, whereas in dark optical lattices the two kinds of contributions subtract. Intuitively, this can be understood by the fact that in bright lattices the atoms are localized at places where their coupling to the light field is strongest, thereby more strongly modifying the refractive index than a homogeneously distributed medium. In dark lattices the atoms tend to minimize their interaction with the trapping field, thus leading to a smaller refractive index. In this case the lattice field will be less sensitive to distortions caused by the atoms.

III. EXPERIMENTAL APPARATUS

In this section we give a description of our experimental system [28]. The preparation of the lattice proceeds in two steps. First, we collect atoms of the rubidium isotope ^{85}Rb for typically 250 ms out of a background vapor by means of a vapor cell magneto-optical trap (MOT) [29]. In the second step, the light beams of the MOT are turned off with a mechanical shutter and the atoms interact for typically 30 ms with the lattice field alone to form the lattice. For convenience, in the experiments presented here the lattice field is not switched off during the filling phase. Only at high intensities of the lattice field does this lead to a degradation of the MOT performance.

A. Magneto-optical trap for ^{85}Rb

The MOT provides us with an atomic sample (almost 10^8 atoms) of high density (some 10^{10} atoms/cm^3) at a relatively low initial temperature (on the order of several tens of μK). The six beams of the light field providing the MOT are slightly tilted with respect to the beams of the optical lattice and aligned such that the atoms collect at exactly the intersection of the MOT and the lattice fields. Both fields are negatively detuned with respect to the closed-cycle hyperfine transition $5S_{1/2}(F=3)\rightarrow 5P_{3/2}(F'=4)$ (F=total angular momentum) of the rubidium D_2 resonance line at $\lambda_L=780.2$ nm. Since atoms might eventually leave this cycle by off-resonant excitation to other hyperfine excited states, a repumping laser beam resonant with a transition from the

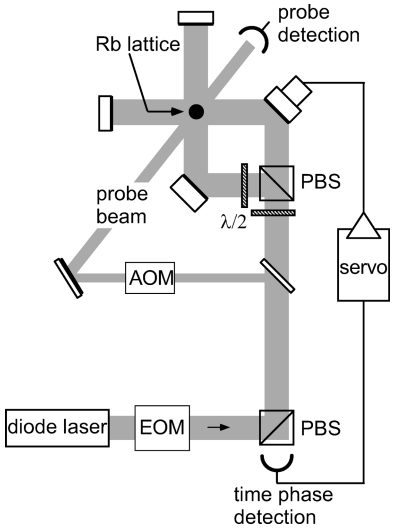

FIG. 5. Experimental setup for the optical lattice.

other hyperfine ground state $5S_{1/2}(F=2)$ to the excited state $5P_{3/2}(F=2,3)$ is coupled into the chamber collinear with the MOT beams. By changing the intensity of the repumping beam we control the number of atoms loaded into the MOT and subsequently into the lattice. Since the rubidium MOT operates in the density limited regime [30] the initial density in the lattice decreases only marginally with decreasing number of trapped atoms. Typical values of the magnetic field gradient are on the order of several Gauss/cm in all experiments presented here. The Earth's magnetic field is carefully compensated by three orthogonal pairs of coils placed along the 40-cm-long sides of a cube.

To provide optical access to the atomic lattice along the directions of Bragg diffraction, we have constructed a stainless steel vacuum chamber with octagonal cross section differing from the chamber used in previous Munich experiments on optical lattices [31]. Indium-sealed high-quality windows are placed at each surface of the chamber (eight windows at the sides of the octagon plus one above and below). The residual pressure of the vacuum system is determined by the rubidium partial pressure of about 10^{-8} mbar and can be increased by heating the rubidium reservoir.

B. Optical lattice at 780 nm

Figure 5 shows a schematic drawing of the lattice field in the horizontal plane. The outcoupled beam (typically 15 mW power) from a grating-stabilized diode laser [32] is spatially filtered and sent through an electro-optic modulator (EOM), which allows fast switching of the lattice field as well as precise adjustment of the intensity. The beam is then split into three orthogonal retroreflected beams ($1/e^2$ diameter $\simeq 5.2$ mm) by means of polarizing beam splitter cubes (PBS) in combination with half-wave plates to adjust the intensity in the individual arms of the lattice field. In the two horizontal x and y branches the same power oscillates while half this value is fed into the vertical z axis. In the horizontal plane both waves are linearly polarized in the plane of propagation, while the standing wave along the vertical axis is right-circularly polarized. In this configuration the potentials are isotropic in the case of the bcc lattice. Piezomounted mirrors control the relative time phase differences between the standing waves. An active stabilization allows us to adjust the phase differences to any desired value, therefore enabling us to switch between different field geometries as described in Ref. [33]. All optical components are cemented to a stainless steel base plate to guarantee high passive stability of the phase differences (drift <10 degrees/min without stabilization) so that a low-frequency servo loop is sufficient to stabilize them.

To create the light shift potentials the frequency of the lattice field is tuned to below the resonance by some linewidths Γ ($\Gamma/2\pi=6$ MHz). In such bright optical lattices polarization gradient forces [2] cool the atoms into the antinodes of the intensity where the light field is purely right-circularly polarized. Thus, the trapped atoms are pumped into the outermost Zeeman sublevel $m_F=+3$ (quantization axis along z) creating a spin polarization of the lattice. In Fig. 2 the two lattice types corresponding to 0° and 90° time-phase difference between the vertical and the horizontal standing waves are depicted. In both cases, the two horizontal linearly polarized waves oscillate with a relative phase difference of 90° leading to a two-dimensional polarization pattern of alternating linear and circular polarization as described in Ref. [34]. The depth of the potential wells and, as a consequence, the energy spacing $\hbar\omega_{\mathrm{vib}}$ of the vibrational levels are functions of the laser detuning from resonance δ and the intensity in the antinodes $\hat{I}$. To a good approximation, we find that the oscillation frequency scales as $\omega_{\mathrm{osc}} \propto \sqrt{\hat{I}/\delta}$ [35]. The laser frequency is stabilized by polarization spectroscopy in a rubidium vapor glass cell at room temperature. Detunings ranging from 0 up to -10Γ can be adjusted with a long-term stability of better than 1 MHz. In our experiments potential depths of up to 10 MHz for the bcc structure and 6 MHz for the st lattice are achieved.

In order to perform probe transmission spectroscopy [36,35] on the bound atoms, a weak linearly polarized probe beam is split from the lattice beam and sent through the atomic sample along the horizontal plane (cf. Fig. 5). Before entering the vacuum chamber the beam is passed through two acousto-optical modulators (AOM, A.A model MTS 1200). The first AOM shifts the frequency by -80 MHz provided by a quartz oscillator (A.A model 80.B46). The second AOM shifts the frequency back by a frequency tunable between $+75$ and $+85$ MHz generated by a voltage-controlled oscillator (Avantek VTO 9020). This allows us to scan the probe frequency around the frequency of the lattice field, while preserving the phase coherence between probe and lattice beam. The transmitted probe intensity is recorded by a photodiode. Probe transmission spectra are taken in real time during the lattice phase (scan time 10 ms). The Raman resonances induced by the probe beam serve as a monitor signal for fine adjustment of the time phase differences and the determination of the oscillation frequency.

C. Laser source at 422 nm

The frequency of the incident light for Bragg scattering is chosen to be close to the $5S_{1/2} \rightarrow 6P_{1/2}$ transition at $\lambda_B = 421.7$ nm, thus enhancing the scattering cross section. The transition has a natural linewidth of only 1.3 MHz. To generate tunable, narrow-band laser light at 422 nm in a simple yet reliable manner we have realized a very compact

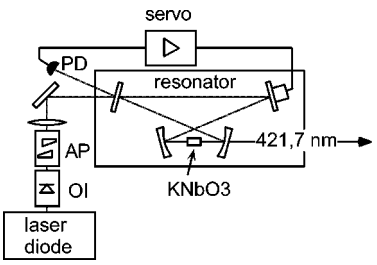

FIG. 6. Compact source of tunable, narrow-band blue laser light. (OI, optical isolator; AP, anamorphic prism pair; PD, phase-sensitive detection.)

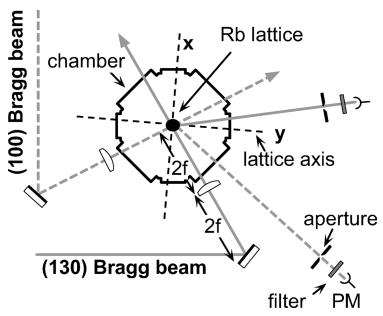

FIG. 7. Experimental geometry for Bragg diffraction from the (100) and (130) planes of the optical lattice.

frequency-doubled diode laser system shown in Fig. 6, which is inspired by a design of Zimmermann *et al.* [37]. It consists of a grating-stabilized laser diode at 843 nm [32] (power 15 mW), which is fed into a small ring resonator in *bow tie* geometry to enhance the power of the fundamental wave. As we shall see later, for some applications in Bragg scattering, e.g., to address all atoms trapped in the optical potentials, it might prove useful to increase the laser bandwidth to values on the order of the potential depth. By simply adding white noise to the injection current (noise generator NoiseCom NC204) we can adjust the linewidth of the blue laser to values from around 1 MHz up to around 10 MHz.

As depicted in Fig. 6 the resonator consists of two curved mirrors (radius 25 mm) separated by 31 mm and two plane mirrors closing the light path yielding a free spectral range of 1770 MHz. One of the plane mirrors has a reflectivity of 96% at 843 nm and serves as an input coupler. All other mirrors are high reflectors for the fundamental wave. The output coupling mirror for the blue light is additionally antireflection coated for 422 nm. The *bow tie* geometry results in two foci. The 6-mm-long nonlinear crystal ($KNbO_3$) with an antireflection coating at 843 nm on both surfaces is placed at the site of the smaller focus located half-way between the curved mirrors (see Fig. 6). The crystal is cut along the crystallographic *a* axis. The fundamental wave is polarized along the *b* axis to benefit from the large nonlinear coupling coefficient d_{23} (in standard notation [38]) for the harmonic wave polarized perpendicular to the fundamental [39]. Phase matching [38] between fundamental and harmonic wave is achieved by stabilizing the crystal temperature to -19 °C by means of a Peltier element that is driven by a PI feedback loop using the current of a temperature sensor as an input signal. The crystal is directly placed onto the Peltier element with heat-conducting grease. To prevent formation of ice at the crystal surfaces the resonator is shielded from air currents by a plastic box purged with nitrogen at very low flux.

A 60-dB optical isolator prevents undesired optical locking of the diode laser to light scattered into the counterpropagating ring cavity mode. A convex lens of 300-mm focal length focuses the diode laser beam onto the larger resonator focus for spatial mode matching. In this way, 70% of the diode laser output power is typically coupled into the cavity. The power of the fundamental wave ($\simeq$10 mW) is enhanced by a factor of 30 inside the resonator, creating up to 600 μW of outcoupled power in the second harmonic in a TEM_{00} mode [40]. The outgoing beam passes through a blue filter to separate the harmonic from the fundamental wave. The resonance of the doubling cavity is actively stabilized to the laser diode frequency by means of a polarization method [41]. We can either scan the blue output frequency up to 4 GHz in 10 ms, or stabilize it to a tunable, low drift Fabry-Pérot etalon to achieve high drift stability over long time periods.

D. Setup for Bragg diffraction

The blue laser beam is split into two independent beams, which are both collimated to a waist w_0 of 2.5 mm by passing through a telescope consisting of two lenses with positive focal length. The diameter $2w_0$ of the beams is thus much larger than the extension of the optical lattice. The resulting divergence $\vartheta=\lambda_B/(\pi w_0)$ is 5.5×10^{-2} mrad. The intensity is attenuated to around 200 μW/cm^2. The low intensity ensures that scattering occurs exclusively into the elastic component of the fluorescence spectrum (pure Rayleigh scattering).

The beams cross the optical lattice in the horizontal plane enclosing an angle of 32.7° and 12.9° with the closest lattice beam, respectively, as shown in Fig. 7. Following Eq. (1) these angles correspond to $\theta_{(100)}=57.3°$ [reflection from the (100) plane] and $\theta_{(310)}=31.3°$ [reflection from the (310) plane] (cf. Fig. 3). In order to vary the incidence angle over several degrees while still keeping the beam centered on the lattice, a mirror is placed inside each telescope such that the outcoupling lens of the telescope images the mirror onto the lattice (see Fig. 7). Fine adjustment of the incidence angle is achieved by a piezocontrolled mirror holder enabling us to scan the incidence angle in the horizontal plane over a range of 2.5 mrad.

The scattered light is detected by photomultipliers (Hamamatsu R928) 60 cm away from the optical lattice at the expected diffraction angles (see Fig. 7). For a typical lattice extension of $D\simeq1$ mm the condition for Fraunhofer diffraction $L\lesssim D^2/\lambda_B$ yields distances L of larger than 2 m between the detector and the lattice. The angular width of the Bragg spot can thus not be directly related to the lattice extension since the size of the diffracted Bragg spot is significantly larger than its diffraction limited size. An iris aperture in front of each photomultiplier covers a detection solid angle of 5×10^{-4} sr chosen much larger than the expected divergence of the diffracted beam. Stray light and fluorescence from the atomic sample at 780 nm are blocked by bandpass filters at 422 nm (bandwidth 10 nm, Anders Optik).

If the incident beam is adjusted according to the Bragg condition we observe a strong increase of the scattered light during the lattice phase as shown in Fig. 8. Since the lattice

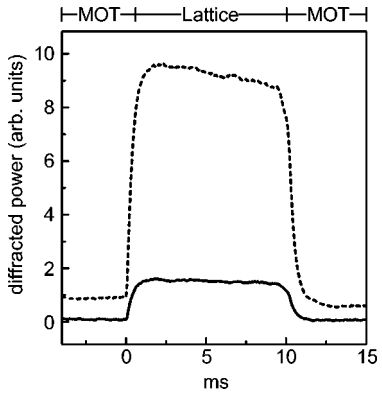

FIG. 8. Total diffracted power during the lattice phase and the loading (MOT) phase for the (100) (dashed line) and the (130) (full line) Bragg spot, respectively. The MOT field is turned off for 10 ms at $t=0$. Fulfillment of the Bragg condition manifests itself in a strong increase of the scattered light into the Bragg directions during the lattice phase. The difference in the diffracted power is due to the different Debye-Waller factors for the two Bragg directions. Some coherent diffraction can also be observed during the loading phase since the lattice field is not turned off then.

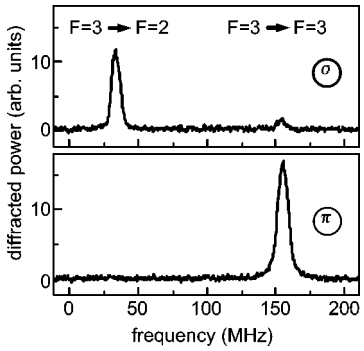

FIG. 9. Spectrum of the Bragg diffracted power vs frequency of the incident blue light. The incident beam is linearly polarized (a) in the horizontal plane (σ polarization) and (b) along the vertical direction (π polarization). The resonance frequencies of the $5S_{1/2}(F=3)\rightarrow 6P_{1/2}(F'=2)$ and $(F'=3)$ transitions are indicated above. The different size of the resonances in (a) reflects the line strength ratio of 1:5. The observed resonance at higher frequencies in (b) for the $F=3\rightarrow F'=3$ transition is about 12 times larger than the corresponding resonance for σ polarization as expected for Rayleigh scattering taking into account the transition matrix elements.

field is present during the loading phase, we find some coherent scattering also during loading, indicating that the lattice field induces a certain degree of long-range order even with the perturbing MOT field present (see Fig. 8). The diffracted power during the MOT phase is strongly dependent on the lattice depth and reaches values of up to one-third of the power diffracted in the lattice phase for the deepest lattices investigated here. If the lattice field is turned off during loading the Bragg diffracted power exceeds the background during the loading phase (MOT field on, lattice field off) by at least three orders of magnitude. To our delight we can watch the Bragg spot, even with unaided eyes, as blue flashes from the atom cloud when looking into the chamber along the Bragg direction.

The oscillator strength of the $5S_{1/2}\rightarrow 6P_{1/2}$ transition is 170 times smaller than the strength of the D_2 line. Absorption of the incoming beams is negligible for the densities we achieve in the lattice even at resonance ($<0.1\%$ for 10^{10} atoms/cm^3). Therefore diffuse scattering of the incident beam need not to be taken into account since all Bragg planes contribute equally to the diffracted signal. This is another important difference from the experiment of Birkl *et al.* [8] where the Bragg beam acted on the strong D_2 line. In that experiment the number of contributing lattice planes was limited due to significant attenuation.

IV. RESULTS

A. Long-range order

One may ask whether the regular structure detected by Bragg diffraction in optical lattices is formed by a spatial density pattern or by a regular spatial modulation of some other atomic observable (e.g., magnetic moment, etc.), or possibly by a mixture of both. We have addressed this question experimentally. In Fig. 9 we show spectra of the diffracted intensity for two orthogonal linear polarizations of the Bragg beam. For the polarization in the horizontal plane [σ polarization, Fig. 9(a)] two resonances appear at the frequencies of the two hyperfine transitions from the $(F=3)$ ground state to the $(F'=2)$ and $(F'=3)$ excited-state levels, respectively. If the polarization is turned by 90° [π polarization, Fig. 9(b)] the most striking feature of the spectrum is the disappearance of the resonance at lower frequency ($F=3\rightarrow F'=2$). Our Bragg diffraction signal must therefore originate from a periodic density distribution $\rho_{m_F=\pm 3}$ of atoms in the $(F=3,m_F=\pm 3)$ ground states since these are the only ones not coupled to the $F'=3$ excited state. The total spatial density distribution of the trapped ground-state atoms $\rho_{\mathrm{tot}}(\mathbf{r})$ can be written as the sum over those of the different Zeeman sublevels m_F: $\rho_{\mathrm{tot}}=\Sigma_{m_F}\rho_{m_F}$. In a pure spin lattice, only certain of the ρ_{m_F} would show long-range order without necessarily implying long-range order in the total distribution ρ_{tot}. From Monte Carlo simulations [42,43] we expect that almost all atoms in the lattice are pumped into the outermost Zeeman sublevel, i.e., $\rho_{\mathrm{tot}}=\rho_{m_F=+3}$. Consequently, our observation of Bragg diffraction reveals the crystalline order of the total density distribution $\rho_{\mathrm{tot}}(\mathbf{r})$.

By blocking the lattice beams along the z axis and keeping the time phase difference for the standing waves in the horizontal plane at the same value ($\phi=90°$) one switches from the spin-polarized bcc lattice to an antiferromagnetic two-dimensional configuration with two face-centered square lattices. The trapping sites for atoms of antiparallel spin are interleaved. For the (10) lattice planes [corresponding to the (100) lattice planes in the three-dimensional case] only the number of available lattice sites is increased by a factor of two, whereas in the (13) direction the spacing between the lattice planes is now decreased by a factor of two. Destructive interference arises in the latter case, and indeed no Bragg diffraction is observed for the (13) direction while the (10) Bragg spot is preserved. This again indicates that the observed Bragg diffraction is due to the regular density distribution of localized atoms.

B. Extension of the lattice

An important quantity to be investigated is the range over which long-range order is preserved. The extension of the

atomic lattice is not necessarily equivalent to the size of the atomic cloud as derived, e.g., from a fluorescence image. It is still an open question how many atoms are actually localized in the lattice and how many form a kind of molasses without periodic order. Section IV D will address this question in more detail. In the ideal case, the maximum size of the lattice should be given by the lattice beam diameters. But perturbations in the phase fronts of the laser beams may distort the lattice field, thus reducing the maximum possible extension.

To determine the diameter of the lattice we measure the total diffracted power P as a function of the incidence angle $\theta_{\rm in}$. The detection solid angle is chosen large compared to the width of the Bragg reflex, which is centered around the angle $\theta_{\mathbf{G}}$ satisfying the Bragg condition for the corresponding $\mathbf{G}$. To calculate $P(\theta_{\rm in})$, we assume a Gaussian probability distribution [44] proportional to $\exp(-4\mathbf{R}^2/D^2)$ for finding an atom at a site $\mathbf{R}$ where we call D the diameter of the lattice that indicates the range over which long-range order is preserved. We neglect any incoherent background terms and obtain

$$\frac{dP}{d\sigma}=N_*^2|A_s|^2\beta^2\exp\left(-\frac{1}{8}(\Delta\mathbf{k}-\mathbf{G})^2D^2\right) \tag{8}$$

by incorporating the Gaussian density distribution into Eq. (3).

If we satisfy the Bragg condition in Eq. (8) we find a Gaussian angular distribution for the diffracted radiation with a diffraction-limited $1/e^2$ width given by $4\lambda_B/\pi D$. Integrating Eq. (8) over the solid angle covered by the detector (which is assumed to be much smaller than 4π but sufficiently large as to completely cover the Bragg peak) yields the diffracted power $P(\theta_{\rm in})$ as a function of the angle of incidence $\theta_{\rm in}$. Varying $\theta_{\rm in}$ in the plane perpendicular to the lattice plane [45] we find to lowest order

$$P(\theta_{\rm in})=N_*^2|A_s|^2\frac{2}{\pi}\left(\frac{\lambda_B}{D}\right)^2\beta^2\exp\left[-8\left(\frac{\theta_{\rm in}-\theta_{\mathbf{G}}}{\Delta\theta_{\rm in}}\right)^2\right], \tag{9a}$$

where the $1/e^2$ angular width $\Delta\theta_{\rm in}$ is given by

$$\Delta\theta_{\rm in}=\frac{4}{\pi}\frac{\lambda_B}{D\,\sin 2\theta_{\mathbf{G}}}, \tag{9b}$$

where we have assumed $\theta_{\mathbf{G}}$ [as given by Eq. (1)] to be significantly larger than λ_B/D ($\lambda_B/D\lesssim 10^{-3}$ in all realistic cases).

Figure 10(a) depicts an example of the dependence of the Bragg diffracted power on the incidence angle. The resulting resonance can be well fitted by a Gaussian. The measured width of the angular resonance is much larger than the divergence angle of the incident beam, which can therefore be neglected. The width of this resonance yields the lattice extension via Eq. (9b).

As described in Sec. III A we change the initial size of the atomic cloud by varying the number of atoms trapped in the MOT. Figure 10(b) shows the diameter of the lattice versus the number of localized atoms, which is determined as will be shown in Sec. IV D. The acceptance angle was measured directly after loading the atoms into the lattice. The corresponding extension of the lattice should therefore coincide

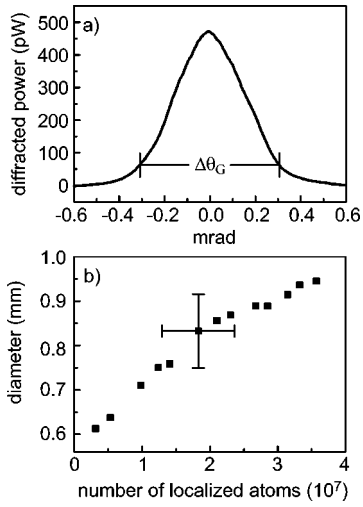

FIG. 10. (a) Diffracted power vs incidence angle for 3.6×10^7 localized atoms. From the acceptance angle $\Delta\theta$ one deduces a lattice diameter of 940 μm. (b) Diameter of the lattice as a function of the number of atoms initially loaded into the lattice. The indicated errors are systematic errors representing the uncertainties in the scaling of the axis.

with the diameter of the atomic cloud in the MOT before it was loaded into the lattice. As expected for a MOT in the density-limited regime the diameter steadily increases with the number of trapped atoms. In all cases the measured size of the atomic lattice is much smaller than the interference pattern of the three standing waves as given by the lattice beam diameters. In addition, we have found no evidence for limitations of the lattice extension due to phase distortions of the lattice field.

After being loaded into the optical lattice the atomic cloud will expand since the strong restoring forces of the MOT are no longer present. By analyzing the temporal evolution of the acceptance angle it is therefore possible to follow the expansion of the lattice and to gain useful information on transport properties in optical lattices [46]. We are currently preparing a study of this phenomenon and the results will be discussed elsewhere.

C. Atomic localization inside the potential wells

Besides the possibility to measure variables concerning global properties of the lattice like the spatial extension, Bragg diffraction gives one the opportunity to investigate average properties of an atom in a single potential well. In particular one may infer information about the mean position spread of the localized atomic wave packets. This is due to the dependence of the Debye-Waller factor on the atomic localization as described by Eq. (4). In principle, it would be possible to deduce the atomic position spread by recording the intensity diffracted into a single Bragg spot [43]. Nevertheless, to minimize experimental uncertainties we employ a more elegant method using Bragg diffraction from two different sets of lattice planes. From Eq. (4) and Eq. (9a) it follows that for larger values of $\Delta\mathbf{k}$ less intensity will be scattered into the Bragg direction for a given atomic position spread. To be able to use the Debye-Waller factor for a quantitative determination of the position spread we have to make

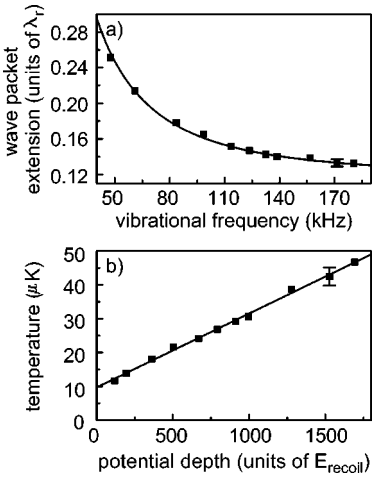

FIG. 11. (a) Mean position spread (rms radius) of the localized atoms vs the oscillation frequency and (b) vibrational temperature vs the potential depth. The indicated errors are representative for all data points.

two assumptions about the energy distribution of the localized atoms. First, the localized atoms have to predominantly occupy low-lying vibrational levels where a harmonic approximation to the potential can be used. For an atomic sample at a typical temperature of some ten μK and optical potentials with a depth of several MHz this should readily be the case. Second, the energy distribution is assumed to be thermal. For bright optical lattices this has been justified by several experiments (see, e.g., [47]).

The sensitivity of different Bragg reflexes on a variation of the atomic localization may differ significantly. This is due to the exponential dependence of the Debye-Waller factor on the rms extension of the localized wave packets δR compared to the spacing of the lattice planes. In our experiment we use the (100) and (130) lattice planes for Bragg diffraction. Given a thermal distribution in isotropic potentials and equal single atom scattering amplitudes the comparison of the total Bragg diffracted powers $P(\theta_{(100)})$ and $P(\theta_{(130)})$ yields the mean absolute value of the atomic position spread. Combining Eqs. (1), (4), and (9a) we get for our choice of lattice planes

$$\delta R = \left(\frac{3\lambda_L^2}{24\pi^2} [\ln P(\theta_{(100)}) - \ln P(\theta_{(130)})] \right)^{1/2}. \quad (10)$$

Since we know the reciprocal lattice vectors we can determine the localization by measuring the total Bragg diffracted powers $P(\theta_{(100)})$ and $P(\theta_{(130)})$. To avoid problems with fluctuations of experimental parameters, such as the number of atoms or the light intensity, we record the two intensities simultaneously as shown in Fig. 8. Care is taken to adjust the intensities in the different arms of the optical lattice and the relative time phases to assure that the resulting 3D potential is isotropic.

Figure 11(a) shows the experimental values of the atomic position spread as determined by means of Eq. (10) versus the vibrational frequency of the optical potentials. The vibrational frequency for each data point is measured by conventional probe transmission spectroscopy as described in Sec. III B. The potential depth was adjusted by varying the intensity of the lattice field while the detuning was kept fixed at -9Γ. One observes a decrease of the position spread δR with increasing vibrational frequency down to a value of $\lambda/7.5$ at a frequency of 180 kHz.

Knowing the mean atomic position spread we can calculate the vibrational temperature in the optical lattice by means of a simple harmonic oscillator model. In an isotropic harmonic potential the relation between position spread and vibrational temperature is given by

$$\delta R = \left(\frac{3\hbar}{2m\omega_{\rm vib}} \coth \frac{\hbar\omega_{\rm vib}}{2k_B T} \right)^{1/2}, \quad (11)$$

with m being the mass of the atom and k_B denoting Boltzmann's constant.

In Fig. 11(b) the corresponding vibrational temperature for each data point in Fig. 11(a) is plotted versus the potential depth U_0 using Eq. (11) and the relation $U_0 = 0.75\omega_{\rm vib}^2/\omega_{\rm recoil}^2$, which is valid for our lattice geometry. The solid curve in Fig. 11(b) is a linear fit to the data points yielding a dependence of the temperature of the form $T = T_0 + \alpha U_0$. By taking the linear functional dependence of T upon the potential depth and using Eq. (11) one obtains the solid curve in Fig. 11(a).

Our finding that the temperature in an optical lattice increases linearly with the potential depth is in qualitative agreement with temperature studies recently performed at NIST by Gatzke *et al.* [47]. In the NIST experiments the temperature of a Cs optical lattice in four beam geometry was deduced from the mean velocity after releasing the atoms from the lattice. In addition, Gatzke *et al.* have determined the position spread of the atomic wave packets in the lattice by heterodyne fluorescence spectroscopy and found it to be independent of the potential depth [47]. This clearly differs from our results as shown in Fig. 11(a) and can mostly be attributed to the fact that T_0 in the Cs lattice is smalller by almost a factor of three. Nevertheless, the dependence of the temperature upon the potential depth given in Ref. [47] implies that the position spread in the Cs lattice should also increase for very shallow lattice potentials. Our method to determine the position spread, i.e., by comparing the intensities diffracted into two different Bragg directions, seems more reliable for shallow potentials. This is due to the fact that our method does not involve the scattering of photons from the lattice field itself, which is naturally reduced in shallow optical lattices.

D. Total number and density of localized atoms

Having determined independently the extension D of the atomic lattice (Sec. IV B) and the Debye-Waller factor β (Sec. IV C) we can now use Eq. (9a) to estimate the number of localized atoms N_* from the measured absolute value of the total diffracted power. This number might differ from the number of atoms initially loaded into the optical lattice because the atoms are spending part of their time in states with very high momentum, i.e., nonlocalized states [46]. Experimental indication for a partition of atoms in nonbound states in optical lattices is reported in Ref. [48]. Measuring the fluorescence or the absorption during the lattice phase yields no information on the fraction of ordered atoms. These mea-

surements do not even provide the total number of atoms since the mean polarization of the nonlocalized atoms is unknown. The power diffracted into a Bragg peak contains no contribution from the nonbound partition and is therefore well suited to investigate this problem. To ensure that all bound atoms contribute to the diffracted signal [49] the laser bandwidth has to be larger than the potential depth. We achieved this by frequency modulation of the diode laser as explained in Sec. III C.

In the following example we calculate the number of localized atoms based on the experimentally determined parameters for the spectrum shown in Fig. 10(a), where the vibrational frequency has been 90 kHz. The scattering amplitude in Eq. (2) contains the atomic polarizability, which we derive from the dipole moment of the transition. For the π polarized incident beam we get the the polarizability $|\alpha| = 3.67 \times 10^{-22}$ m^3. For a lattice with an extension of $D = 0.95 \pm 0.01$ mm and an atomic position spread of $\delta R = (0.171 \pm 0.008)\lambda_L$ we measure a total power diffracted from the (100) plane of $P_{\theta_{(100)}} = (470 \pm 190)$ pW. Uncertainties in the absolute calibration of our photmultipliers mainly contribute to the estimated error. The intensity of the incoming beam was (236 ± 24) μW/cm^2, uniformly distributed over a frequency interval of 10 ± 3 MHz. Since the linewidth of the transition equals 1.3 MHz, we assume an effective intensity of 31 ± 10 μW/cm^2 for the calculation of the scattering amplitude. Equation (9a) yields $(3.6 \pm 1.1) \times 10^7$ as the number of localized atoms. This has to be compared with the number of almost 10^8 atoms trapped in the MOT, which we deduced from the fluorescence during the MOT phase assuming random distribution of population among the Zeeman sublevels.

It becomes obvious that the large systematical errors relating the measured power to the absolute number of atoms impede a clear statement on the actual fraction of atoms localized in the potential wells. Furthermore, at the present state of our experiment we can provide no reliable estimate on the transfer efficiency from the MOT into the lattice. However, since the diffracted power scales as N_*^2 [cf. Eq. (9a)] it provides an excellent signal for comparing the (relative) number of localized atoms. This is used in the experiments concerning the backaction of the atoms on the lattice field which are described Sec. IV F.

E. Probe-induced resonances

Several techniques have been demonstrated to investigate the atomic motion inside the potential wells [13,14,10]. Probe transmission spectroscopy has been proven to be a particularly convenient way. When the frequency difference between the probe and the lattice fields matches the separation between two vibrational states, photons are exchanged between both fields due to stimulated Raman transitions between different vibrational states [36]. Since the atoms are bound at points of pure σ^+ polarization the probe polarization has to lie in the horizontal plane (σ polarization) to only couple vibrational levels in the $m_F = +3$ potential via stimulated Raman transitions involving one photon from each of the lattice field and the probe. As shown in Fig. 12(a), these transitions lead to amplifying (absorbing) resonances in the probe transmission when the probe frequency is below

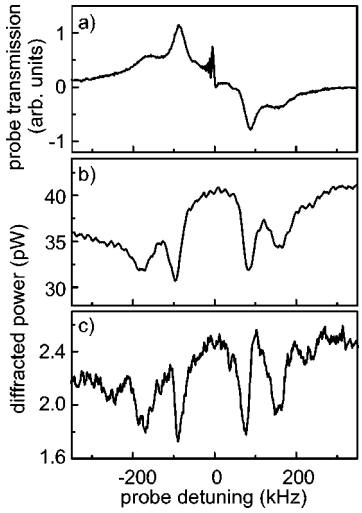

FIG. 12. Probe-induced resonances in (a) the probe transmission, and the power diffracted from the (b) (100) and the (c) (130) lattice planes. The resonances yield an oscillation frequency for the potential wells of 90 kHz. The resonances in the Bragg spectra are much narrower and show less anharmonicity. In the (130) spectrum even the third sidebands can be identified.

(above) the lattice field frequency since lower-lying vibrational levels are more populated than higher-lying ones.

From the positions of the first resonances in the transmission spectra we extract the oscillation frequency along the probe beam and thus determine the depth of the potential wells. The probe transmission spectrum therefore allows one to clearly distinguish between different time phase differences of the lattice field, which result in different potential depths. However, a quantitative analysis of the spectra becomes a difficult issue since *all* populated bound levels contribute to the signal. Higher-lying, i.e., less tightly bound states, experience a large anharmonicity. Although these states are less populated than the low-lying states, they contribute significantly to the Raman signal because of their larger transition matrix elements (Franck-Condon overlap) [34]. Extracting quantitative information about the temperature or the position spread in the lattice is therefore quite difficult if not impossible.

The dependence of the Debye-Waller factor on the position spread of the bound atoms can be utilized for a combination of probe spectroscopy with Bragg scattering. In a classical picture the time varying interference pattern between the probe and the lattice field parametrically drives the oscillatory motion of atoms bound in the potential wells. This process becomes resonant when the interference pattern oscillates at the atom's vibrational frequency. The amplitude of the atomic motion is increased along the direction $\mathbf{u}$ of the probe beam leading to an increase of $\delta R_{\mathbf{u}}$. Quantum mechanically, probe-induced Raman transitions are accompanied by a population transfer from a lower, more strongly populated vibrational level to a higher, less populated one. As a consequence, the Raman process always increases the mean spatial extension of the atomic c.m. wave function along the probe beam, i.e., $\delta R_{\mathbf{u}}$ in Eq. (4) increases. From Eq. (3) it follows that the power diffracted into a Bragg spot must decrease. Due to the exponential dependence of the Debye-Waller factor on the localization, mainly population

changes of low-lying bound states manifest themselves in the decrease of the Bragg diffracted power.

The effect is demonstrated in Fig. 12 where we have scanned the weak probe beam while simultaneously recording the transmitted probe power at 780 nm, and the total Bragg diffracted power at 422 nm for both the (100) and the (130) Bragg reflex, respectively. The resonances in the diffracted signal are much narrower than the corresponding resonances in the probe transmission spectrum (at 780 nm), particularly for the second Raman side band near $\pm 2\omega_{\mathrm{vib}}$. Furthermore, the resonances at 422 nm exhibit much less anharmonicity, seen by the fact that the second sidebands appear almost exactly at $\pm 2\omega_{\mathrm{vib}}$. In order to check whether these resonances are induced by an increase of the wave-packet extension along the probe direction we have repeated the experiment with the probe beam perpendicular to the (130) lattice vector. In this case the Debye-Waller factor [Eq. (4)] for the (130) direction is not modified by the probe ($\delta R_{\mathbf{u}}=0$), and we indeed observe that the probe-induced resonances in the (130) Bragg spot do not appear.

These observations confirm that mainly the lowest bound states yield a significant contribution to the probe-induced Bragg spectrum. This selectivity gets more pronounced if the spacing of the lattice planes for Bragg diffraction is smaller. This explains why even third-order sidebands are distinguishable in the probe-induced spectrum of the (130) reflex shown in Fig. 12(b).

The selectivity of the probe-induced resonances on atoms deeply bound in the potential wells also becomes apparent when we heat the lattice by tuning the lattice field closer to resonance. In this case, most of the population is transferred to higher-lying vibrational states. The Bragg spectrum vanishes while the probe transmission spectrum is still preserved but shows significantly broadened Raman resonances, indicating that atoms are still bound in the lattice.

F. Modification of the lattice constant due to atomic backaction

From our discussion in Sec. II C it follows that variations in the density of trapped atoms change the refractive index, which, for red detuned optical lattices, becomes apparent in a shrinking of the lattice structure as a whole. This contraction should show up as a minute deviation of the measured Bragg angle from the one calculated without including the backaction of the atoms on the lattice field [Eq. (1)]. By recording the total Bragg diffracted power versus the angle of incidence (as described in detail in Sec. IV B) for different values of the atomic density one is thus able to measure the corresponding change of the lattice constant.

To vary the density the lattice is filled at a maximum density limited by the MOT (remember that the MOT is operated in the density-limited regime). We then let the lattice expand for approximately 100 ms, which naturally leads to a decrease of the density. During this interval a series of angular spectra is recorded. For every spectrum the Bragg angle is determined to within better than 10 μrad by fitting a Gaussian to the spectrum. This means that we are sensitive to changes of the lattice spacing as small as ~ 5 pm. The number of trapped atoms is determined for each individual spectrum as described in Sec. IV D. By means of Eq. (9b) the diameter D of the atomic sample is deduced from the width

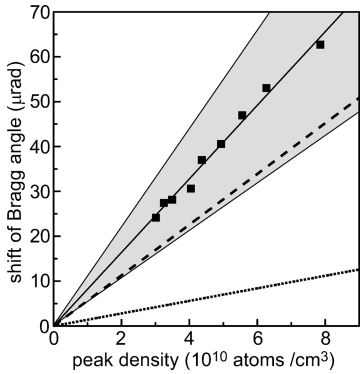

FIG. 13. Shift of the Bragg angle as a function of density. The solid line is a linear fit to our data. The shaded area represents a confidence interval for this fit including the uncertainties of the density measurement and the calibration of the Bragg angle. The uncertainties as indicated are mainly due to the error in determining the density and to a lesser extent to the calibration of the Bragg angle. The dashed line marks the expected change of the Bragg angle including the enhancement due to the localization of the atoms ($\delta R=0.18\lambda_L$) in an ordered lattice, while for the dotted line this enhancement is discarded.

of the angular spectra, which, together with the number of atoms N_*, yields the peak density $\varrho_0=N_*/[(\sqrt{\pi}/2)D]^3$ of the Gaussian density distribution $\varrho(\mathbf{r})=\varrho_0\exp(-4\mathbf{r}^2/D^2)$. Thus, the series of angular spectra represents a self-consistent data set providing the Bragg angle versus the peak density.

The result is shown in Fig. 13 for an optical lattice with a vibrational frequency of 80 kHz. The Bragg angle increases linearly with the density as expected from Eq. (5), which proves that the spacing between the (100) lattice planes has actually decreased. At the highest densities the measured change of the Bragg angle can be directly translated into an average reduction of the lattice spacing $d_{(100)}\simeq 390$ nm by 40 pm.

In general, the nonuniform density distribution in the optical lattice leads to a variation of the lattice spacing over the atomic sample. Similar to the Debye-Waller factor, a nonuniform distribution of lattice spacings essentially leads to a decrease of the Bragg diffracted signal. However, this effect can be neglected with respect to the Debye-Waller factor since the average reduction of the lattice spacing is much smaller than the mean position spread of the localized atoms ($\delta R\sim 140$ nm).

To answer the question whether there are identifiable effects of the atomic localization on the observed shift of the Bragg angle we specialize Eq. (7) to the case of our six beam bright optical lattice introduced in Sec. III B. We write $\vec{\vec{\alpha}}_{\mathbf{R}}$ in terms of its components $\alpha_{(+)}$ and $\alpha_{(-)}$ for σ^+ and σ^- polarized light, respectively. We expect two types of coherent scattering contributions, i.e., backward scattering and 90° angle scattering which scale with two different Debye-Waller factors $\beta_0=\exp(-\frac{2}{3}k_L^2\delta R^2)$ and $\beta_{90}=\exp(-\frac{1}{3}k_L^2\delta R^2)$. For the index of refraction experienced by either of the waves propagating within the xy plane we obtain

$$n_{xy}-1=\tfrac{1}{4}\varepsilon_0\varrho[(1+\beta_0+4\beta_{90})\alpha_{(+)} + (1+\beta_0-2\beta_{90})\alpha_{(-)}]. \qquad (12a)$$

The sign in front of the Debye-Waller factors stems from the constructive and destructive interference, respectively, of the σ^+ and σ^- components of the lattice beams at the location **R**. Because the trapped atoms are assumed to be completely optically pumped into the outermost Zeeman component we may assume that $\alpha_{(+)}$ is considerably larger than $\alpha_{(-)}$ and Eq. (12a) reduces to its first term. Similarly, we find that the index of refraction for either of the circularly polarized lattice beams along the z axis is given by

$$n_z - 1 = \tfrac{1}{4}\varepsilon_0 \varrho (1 + \beta_0 + 4\beta_{90})\alpha_{(+)}. \tag{12b}$$

If two classes of lattice sites exist as in antiferromagnetically ordered optical lattices [34,8] the preceeding analysis can be easily extended by treating both lattices independently and summing over the corresponding contributions. One can then apply our model to the four-beam field configuration used in the Bragg experiment in Gaithersburg [8]. We find $n-1=\frac{1}{2}\varepsilon_0\varrho(1+3\beta_{90})(\alpha_{(+)}+\alpha_{(-)})$, which reproduces the result used in Ref. [8].

To apply Eq. (12) to the nonuniform density distribution in our experiment we replace the density ϱ by the average density $\overline{\varrho}$ defined by $\overline{\varrho} \equiv \int \varrho^2 d^3\mathbf{r} / \int \varrho d^3\mathbf{r}$. For a Gaussian distribution, the average density is related to the peak density by $\overline{\varrho} = \varrho_0 / 2\sqrt{2}$. The Debye-Waller factors β_0 and β_{90} are calculated by taking the position spread from the data presented in Sec. IV C. For the vibrational frequency of 80 kHz we measured $\delta R = 0.18\lambda_L$ and thus $n-1$ is expected to be enhanced by a factor of $\simeq 4$ as compared to the value for a disordered gas ($\beta_0=\beta_{90}=0$) at the same density. In Fig. 13 we have plotted the shift of the Bragg angle as a function of density as expected from Eq. (12). In one case we have neglected the contribution of the localization to the refractive index (dotted line), in the other case we have included the actual position spread (dashed line). The corresponding calculated values for the angle shifts are 1.4×10^{-16} cm$^3\varrho_0$ without and 5.6×10^{-16} cm$^3\varrho_0$ with taking into account the enhancement due to the localization of the atoms in the lattice. Within the experimental uncertainties given by the shaded area in Fig. 13, our data thus show clear evidence for the enhancement of the refractive index due to the strong localization of the atoms.

V. DISCUSSION

Bragg diffraction has opened new insights into the properties of light bound atomic lattices. We have demonstrated an *in situ* method which provides a powerful diagnostic tool for their characterization (extension of the long-range order, position spread of the bound wave packets, number of ordered atoms). One can now search for additional correlations in the spatial density distribution of the atoms which may, e.g., indicate optical binding [24]. In view of the reasonable experimental effort our method may also prove useful for applications in atom lithography employing optical lattices [50,51].

The direct determination of the Debye-Waller factor from the comparison of two different Bragg spots enables one to measure the position spread of the atomic wave packet in real time. This offers the opportunity to aim for nonclassical parametric motion in the potential wells (''breathing modes'') [42]. Results on oscillations in the position spread after nonadiabatic changes of the potential have recently been observed by us [17] and independently by other groups [52–54].

The interpretation of our data was based on a simple model assuming a thermal distribution of population among the vibrational states. This assumption has been proven reasonable for bright optical lattices, but it breaks down in the case of dark optical lattices [15]. Evidence for a nonthermal distribution has already been given since most of the population is found in the vibrational ground state [55,56]. In this case, our model may still be applied since the contribution of the small partition in higher bound states does not significantly contribute to the diffraction signal due to their large position spread. The extension of the wave packet in Eq. (4) then has to be replaced by the ground-state extension resulting in a better localization and thus a larger Debye-Waller factor as compared to bright optical lattices.

Since Bragg diffraction relies on elastic Rayleigh scattering from the localized atoms it is especially suited as a nondestructive detection method for the new kind of optical lattices in far-detuned fields, which have recently been demonstrated [56–59]. Conventional probe transmission is not suited here since the large detuning of the lattice field results in very small Raman transition rates, and characterization methods employed up to now have been destructive.

Directly after loading the atoms into the lattice one may follow the formation of long-range order by observing a temporal increase of the Bragg signal. By monitoring the acceptance angle as a function of time it will be possible to study atomic transport in optical lattices. Spatial diffusion is predicted to be anomalous (*Lévy flights*) for certain lattice parameters [46]. Previous experiments seem to indicate such non-Brownian atomic diffusion [10]. Another approach to diffusion processes in optical lattices might be the investigation of intensity correlations in Bragg diffracted light. Time scales during which the atoms are bound at a particular site before hopping to another well should become apparent. An experiment along these lines was recently published investigating atomic transport in optical lattices through intensity correlations in the fluorescence [60]. Similar experiments employing Bragg-diffraction would promise much increased signal to noise.

On the other hand, fundamental processes in the light-matter interaction can be studied. As an example, we have demonstrated how the presence of localized atoms modifies the index of refraction and thus the lattice constant. Our model described the localized atoms as a medium with an effective refractive index taking into account only lowest-order scattering theory. Yet it is still unclear how mutual interactions between the atoms might modify the lattice structure and the long-range properties of optical lattices. It seems possible to enter the regime of multiple light scattering by operating dark optical lattices at high filling rates which will offer an intriguing application of Bragg scattering in the search for such modifications of the lattice structure. In this regime, the periodic arrangement of cold atoms in the near resonant light field also provides a unique model system suited to search for photonic band gaps [26,61].

ACKNOWLEDGEMENTS

We are grateful to Tilman Esslinger and Claus Zimmermann for many enlightening discussions. This work was supported in part by the German-Israeli Foundation for Scientific Research and Development under Grant No. I-216.07/91, and the German BMBF under Contract No. 13N6637/5.

[1] P. S. Jessen and I. H. Deutsch, Adv. At., Mol., Opt. Phys. **37**, 95 (1996), and references therein.

[2] J. Dalibard and C. Cohen-Tannoudji, J. Opt. Soc. Am. B **6**, 2023 (1989).

[3] Y. Castin and J. Dalibard, Europhys. Lett. **14**, 761 (1991).

[4] D. R. Meacher, S. Guibal, C. Mennerat, J.-Y. Courtois, K. I. Petsas, and G. Grynberg, Phys. Rev. Lett. **74**, 1958 (1995).

[5] S. Guibal, C. Mennerat-Robilliard, D. Larousserie, C. Triche, J. Y. Courtois, and G. Grynberg, Phys. Rev. Lett. **78**, 4709 (1997).

[6] L. Guidoni, C. Triche, P. Verkerk, and G. Grynberg, Phys. Rev. Lett. **79**, 3363 (1997).

[7] M. Ben Dahan, E. Peik, J. Reichel, Y. Castin, and C. Salomon, Phys. Rev. Lett. **76**, 4508 (1996); S. R. Wilkinson, C. F. Bharucha, K. W. Madison, Q. Niu, and M. G. Raizen, *ibid.* **76**, 4512 (1996).

[8] G. Birkl, M. Gatzke, I. H. Deutsch, S. L. Rolston, and W. D. Phillips, Phys. Rev. Lett. **75**, 2823 (1995).

[9] M. Weidemüller, A. Hemmerich, A. Görlitz, T. Esslinger, and T. W. Hänsch, Phys. Rev. Lett. **75**, 4583 (1995).

[10] A. Hemmerich, M. Weidemüller, and T. W. Hänsch, Europhys. Lett. **27**, 427 (1994).

[11] Experimental data for the four-wave-mixing process can also be found in B. Lounis, thèse de doctorat, Université Paris XI, Paris, 1993 (unpublished).

[12] The connection between four-wave mixing and Bragg diffraction is discussed in A. Görlitz, T. W. Hänsch, and A. Hemmerich, J. Mod. Opt. **44**, 1853 (1997).

[13] P. Verkerk, B. Lounis, C. Salomon, C. Cohen-Tannoudji, J.-Y. Courtois, and G. Grynberg, Phys. Rev. Lett. **68**, 3861 (1992).

[14] P. S. Jessen, C. Gerz, P. D. Lett, W. D. Phillips, S. L. Rolston, R. J. C. Spreeuw, and C. I. Westbrook, Phys. Rev. Lett. **69**, 49 (1992).

[15] A. Hemmerich, M. Weidemüller, T. Esslinger, C. Zimmermann, and T. W. Hänsch, Phys. Rev. Lett. **75**, 37 (1995).

[16] R. J. C. Spreeuw, T. Pfau, U. Janicke, and M. Wilkens, Europhys. Lett. **32**, 469 (1995).

[17] A. Görlitz, M. Weidemüller, T. W. Hänsch, and A. Hemmerich, Phys. Rev. Lett. **78**, 2096 (1997).

[18] N. W. Ashcroft and N. D. Mermin, *Solid State Physics* (Saunders, Philadelphia, 1976).

[19] Crystallography of different types of optical lattices is presented by K. I. Petsas, A. B. Coates, and G. Grynberg, Phys. Rev. A **50**, 5173 (1994).

[20] J. M. Cowley, *Diffraction Physics*, 2nd ed. (North-Holland, Amsterdam, 1981), p. 144.

[21] A. Guinier, *X-Ray Diffraction* (Freeman, San Francisco, 1963), p. 193.

[22] The same reasoning also holds if the distribution is nonthermal but δR is small compared to λ_L. The Debye-Waller factor can then be written as $\beta \simeq 1 - W$ with W given by Eq. (4).

[23] A. Hemmerich, M. Weidemüller, T. Esslinger, and T. W. Hänsch, Europhys. Lett. **21**, 445 (1993).

[24] M. M. Burns, J.-M. Fournier, and J. A. Golovchenko, Science **249**, 749 (1990).

[25] D. Sesko, T. Walker, and C. E. Wieman, J. Opt. Soc. Am. B **8**, 946 (1989).

[26] I. H. Deutsch, R. J. C. Spreeuw, S. L. Rolston, and W. D. Phillips, Phys. Rev. A **53**, R3727 (1996).

[27] The field from such a dipole sheet is derived in M. Sargent, M. O. Scully, W. E. Lamb, *Laser Physics* (Addison-Wesley, Reading, MA, 1973), Appendix A.

[28] For further details see M. Weidemüller, MPQ Report No. 202 (MPI für Quantenoptik, Garching, 1995).

[29] C. Monroe, W. Swann, H. Robinson, and C. Wieman, Phys. Rev. Lett. **65**, 1571 (1990).

[30] C. G. Townsend, N. H. Edwards, C. J. Cooper, K. P. Zetie, C. J. Foot, A. M. Steane, P. Szriftgiser, H. Perrin, and J. Dalibard, Phys. Rev. A **52**, 1423 (1995).

[31] A review of our previous work is presented in A. Hemmerich, M. Weidemüller, and T. W. Hänsch, in *Coherent and Collective Interactions of Particles and Radiation Beams*, International School of Physics ''Enrico Fermi,'' Course CXXXI, edited by R. Bonifacio, W. Barletta, and A. Aspect (IOS Press, Amsterdam, 1996).

[32] L. Ricci, M. Weidemüller, T. Esslinger, A. Hemmerich, C. Zimmermann, V. Vuletic, W. König, and T. W. Hänsch, Opt. Commun. **117**, 541 (1995).

[33] A. Hemmerich, D. Schropp, and T. W. Hänsch, Phys. Rev. A **44**, 1910 (1991).

[34] A. Hemmerich and T. W. Hänsch, Phys. Rev. Lett. **70**, 410 (1993).

[35] A. Hemmerich, M. Weidemüller, and T. W. Hänsch, Laser Phys. **4**, 884 (1994).

[36] J.-Y. Courtois and G. Grynberg, Phys. Rev. A **46**, 7060 (1992).

[37] C. Zimmermann, V. Vuletic, A. Hemmerich, and T. W. Hänsch, Appl. Phys. Lett. **66**, 2318 (1995).

[38] G. D. Boyd, *Nonlinear Optics* (Academic Press, San Diego, 1992).

[39] J.-C. Baumert, P. Günther, and H. Melchior, Opt. Commun. **48**, 215 (1983).

[40] The distances between the curved mirrors have been adjusted such that the focus is the same in the sagittal and in the tangential plane yielding a round output beam.

[41] T. W. Hänsch and B. Couillaud, Opt. Commun. **35**, 441 (1980).

[42] S. Marksteiner, R. Walser, P. Marte, and P. Zoller, Appl. Phys. B: Lasers Opt. **60**, 145 (1995).

[43] G. Raithel, G. Birkl, A. Kastberg, W. D. Phillips, and S. L. Rolston, Phys. Rev. Lett. **78**, 630 (1997).

[44] The assumption, that the spatial distribution of atoms in our optical lattice is Gaussian, seems well justified, since the lattice is loaded from a conventional MOT and hence the spatial distribution in the lattice should reflect the spatial distribution in the MOT.

[45] Changing θ_{in} along the lattice plane does to lowest order not change the diffracted power.
[46] S. Marksteiner, K. Ellinger, and P. Zoller, Phys. Rev. A **53**, 3409 (1996); W. Greenwood, P. Pax, and P. Meystre, *ibid.* **56**, 2109 (1997).
[47] M. Gatzke, G. Birkl, P. S. Jessen, A. Kastberg, S. L. Rolston, and W. D. Phillips, Phys. Rev. A **55**, R3987 (1997).
[48] A. Kastberg, W. D. Phillips, S. L. Rolston, R. J. C. Spreeuw, and P. S. Jessen, Phys. Rev. Lett. **74**, 1542 (1995).
[49] This effect had been underestimated in our previous analysis given in Ref. [9]
[50] G. Timp, R. E. Behringer, D. M. Tennant, J. E. Cunningham, M. Prentiss, and K. K. Berggren, Phys. Rev. Lett. **69**, 1636 (1992).
[51] J. J. McClelland, R. E. Scholten, E. C. Palm, and R. J. Celotta, Science **262**, 877 (1993).
[52] G. Raithel, G. Birkl, W. D. Phillips, and S. L. Rolston, Phys. Rev. Lett. **78**, 2928 (1997).
[53] P. Rudy, R. Ejnisman, and N. P. Bigelow, Phys. Rev. Lett. **78**, 4906 (1997); R. Ejnisman, P. Rudy, H. Pu, and N. P. Bigelow, Phys. Rev. A **56**, 4331 (1997).
[54] M. Kozuma, N. Nakagawa, W. Jhe, and M. Ohtsu, Phys. Rev. A **57**, R24 (1998).
[55] T. Esslinger, F. Sander, A. Hemmerich, T. W. Hänsch, H. Ritsch, and M. Weidemüller, Opt. Lett. **21**, 991 (1996).
[56] T. Müller-Seydlitz, M. Hartl, B. Brezger, H. Hänsel, C. Keller, A. Schnetz, R. J. C. Spreeuw, T. Pfau, and J. Mlynek, Phys. Rev. Lett. **78**, 1038 (1997).
[57] B. P. Anderson, T. L. Gustavson, and M. A. Kasevich, Phys. Rev. A **53**, R3727 (1996).
[58] D. L. Haycock, S. E. Hamann, G. Klose, and P. S. Jessen, Phys. Rev. A **55**, R3991 (1997).
[59] S. Friebel, C. D'Andrea, J. Walz, M. Weitz, and T. W. Hänsch, Phys. Rev. A **57**, R20 (1998).
[60] C. Jurczak, B. Desruelle, K. Sengstock, J.-Y. Courtois, C. I. Westbrook, and A. Aspect, Phys. Rev. Lett. **77**, 1727 (1996).
[61] D. V. van Coevorden, R. Sprik, A. Tip, and A. Lagendijk, Phys. Rev. Lett. **77**, 2412 (1996).